

Impact of synthesis conditions on meso- and macropore structures of resorcinol–formaldehyde xerogels

Ahmed Awadallah-F · Ahmed M. Elkhatat ·
Shaheen A. Al-Muhtaseb

Received: 28 April 2011 / Accepted: 26 June 2011 / Published online: 7 July 2011
© Springer Science+Business Media, LLC 2011

Abstract Xerogels were prepared by the sol–gel polymerization of resorcinol with formaldehyde at different conditions. The effects of different synthesis factors (namely, resorcinol-to-formaldehyde ratio, resorcinol-to-water ratio, resorcinol-to-catalyst ratio, and initial solution pH) on the surface areas, pore volumes, pore size distributions, and adsorption capacity of liquid nitrogen were studied. Factorial design was also used to investigate the relative significance of these factors on the resulting xerogels properties, and the possible interactions between them. The mean effects of the most significant factors and factor interactions on determining the pore structures and adsorption capacities were evaluated. The synthesized xerogels were characterized by Fourier transmission infrared spectroscopy, thermal gravimetric analysis, scanning electron microscopy, and surface area analyzer. The results showed that surface areas, pore size distributions, and nitrogen adsorption capacity are dependent completely on the recipes used to prepare the xerogels. Pore structure results put xerogel samples as candidates for adsorption technology, ultra-filtration, and nano-filtration fields based on pore sizes and pore volume scales.

Introduction

Organic gel materials are widely used in adsorption and separation technologies. Adsorption and separation processes rely mainly on the pore structure of the adsorbent material, among other factors. It is noticeable that organic gels present some advantages over conventional inorganic gels, such as higher stability in acidic and basic media [1]. Conventional inorganic gels such as alumina and silica dissolve at high solution pH and the former is also attacked even at very low solution pH [1]. Resorcinol–formaldehyde (RF) resins are among the most famous organic gels. RF resins have been extensively studied over the past two decades, since their introduction by Pekala [2]. RF gels prepared using water as a solvent can be dried by various methods such as supercritical drying (aerogels), freeze-drying (cryogels), and evaporative drying under vacuum or atmospheric pressures (xerogels) [3]. Of the three drying methods outlined above, supercritical drying is the most useful method for obtaining mesoporous RF gels, but the associated drying procedure is sophisticated and costly. With freeze-drying, which is also an effective way of preparing cryogel with high surface area and controlled pore structure, the drying step is much less expensive [4]. Moreover, the surface area, pore volume, and mean pore diameter are largest for RF cryogels [5]; and the shrinkage is also the lowest. Although both supercritical drying and freeze-drying methods are efficient for fabricating dried organic porous materials, these methods are rather expensive and difficult to handle. As to the third method, drying by an inert atmosphere is the simplest way to convert wet RF gels into dry xerogels that can be used practically in various applications. However, the surface area, pore volume, and mean pore diameter of xerogels are smaller than those of the aerogels or the cryogels. Nonetheless, the

A. Awadallah-F · A. M. Elkhatat · S. A. Al-Muhtaseb (✉)
Department of Chemical Engineering, Qatar University,
P.O. Box 2713, Doha, Qatar
e-mail: s.almuhtaseb@qu.edu.qa

A. Awadallah-F
National Center for Radiation Research and Technology,
P.O. Box 29, Nasr City, Cairo, Egypt

shrinkage ratios and final pore structures of the xerogels depend on the synthesis conditions of the wet gel itself [5]. Therefore, the choice of drying at ambient pressure has been suggested as an alternative gel drying process by many investigators [2, 3]. This method is considered among the methods that have been suggested to overcome the disadvantages of other costly and uneasy to handle methods [6–8].

Therefore, the drying method used in the gel preparation exerts a strong influence on the final structure of the dried gel, and hence on its corresponding performance in adsorption and various separations. Activated carbons made from organic gels, especially RF gels, attract the attention of separation specialists [9] for many adsorption applications. Furthermore, the high specific surface areas and electric conductivities obtained make these materials good candidates for the elaboration of electrodes for super capacitors [10], batteries, or fuel cells [11]. Similarly, the low thermal conductivities observed are interesting for the development of thermal insulators [12]. These attractive properties are mainly results of the outstanding pore structure characteristics of these materials. It is noteworthy that the pore structures of RF xerogels are completely based on (i) drying methods, (ii) solvent species used in the solvent exchange, and (iii) synthesis recipes used in their polymerization reaction [13]. The mechanism of the polymerization reaction of resorcinol and formaldehyde is shown in Fig. 1 [14]. This reaction system is governed by an addition–condensation reaction mechanism [15], which is close to the mechanisms encountered for the synthesis of inorganic sol–gels such as silica or titanium based systems [16]. Therefore, RF gel pore structures are also affected by the pH of synthesis media. Lower initial solution pH corresponds to RF xerogels with higher surface areas and pore volumes, and also broader pore size distributions [17]. Adsorption is a very important field in chemical and petrochemical industries. According to the IUPAC recommendation [16], porous materials are characterized mainly by the presence of three types of pore sizes: micropores (<2 nm), mesopores (2–50 nm), and macropores (>50 nm). Characterizing the pore structures of RF gels is an important aspect of understanding the synthesized materials and their various potential applications. Investigating these gels according to the corresponding pore structure can indicate which separation applications these gels are suitable for.

To the knowledge of the authors, there is only one published article which investigated the pore structures of organic gels [11]. However, that article did not take into account the multi-factor effect of synthesis parameters on the pore structure. It is worthwhile to state that a factorial design experiment had been previously designed and carried out [18] to determine the collective effects of the

initial solution pH, weight percentage of solids, pyrolysis temperature and gel type on the surface area, pore volume, and electrochemical double-layer capacitance of RF carbon gels. That article gave an overall image of the most and least effective factors and factor interactions which determine the pore sizes and surface areas of carbon gels. Other works also addressed the effects of various synthesis parameters on the characteristics of RF carbon gels [19, 20].

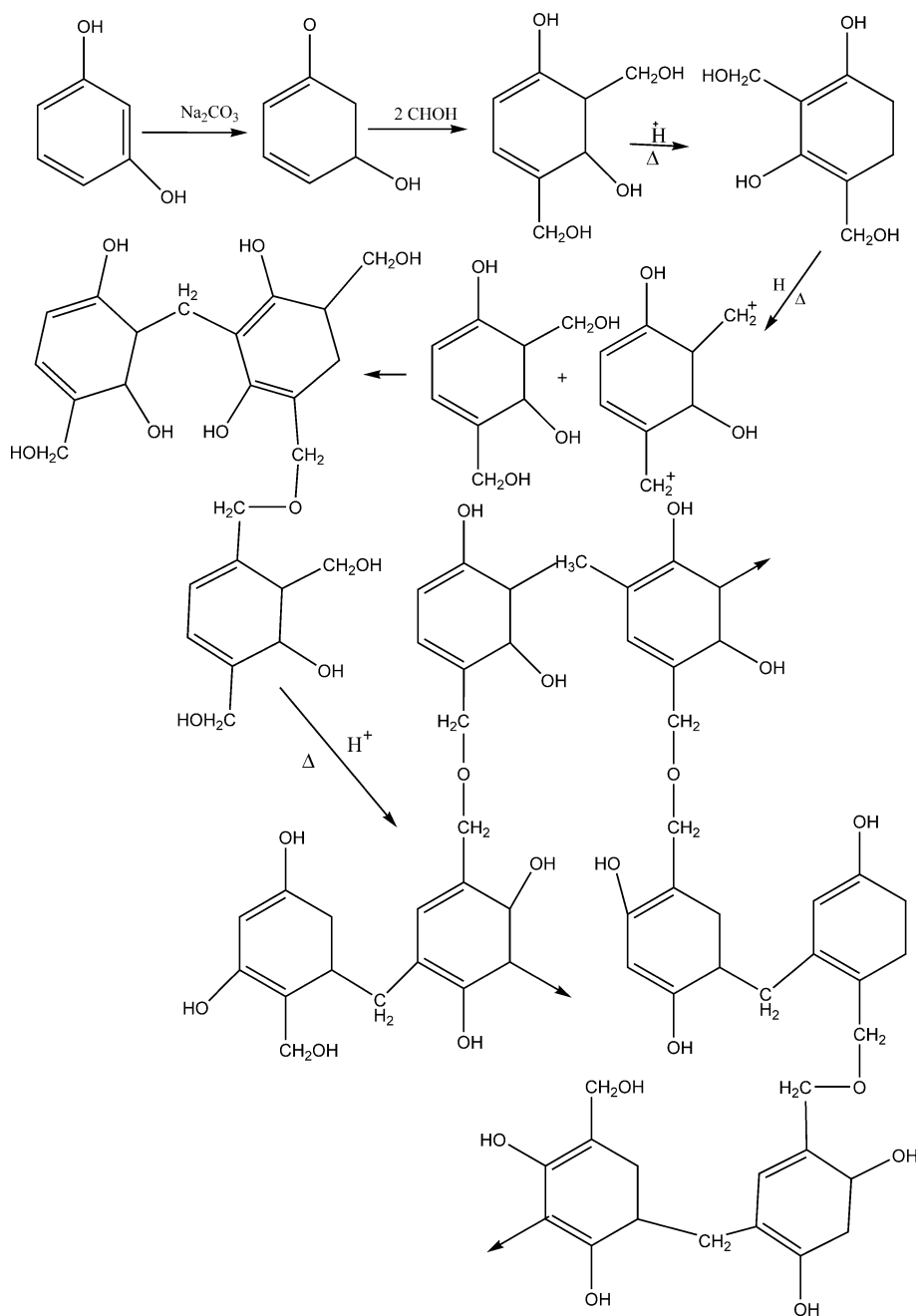
In this study, a factorial design of experiments approach is designed to investigate the collective effects of different synthesis factors on the structures of RF organic xerogels. Various synthesis recipes resulted from the factorial design of experiments approach to cover the effects of such factors and conditions (including the initial solution pH and the molar ratios of resorcinol-to-formaldehyde (R/F), resorcinol-to-catalyst (R/C), and resorcinol-to-water (R/W)) on the final properties of the organic xerogels (i.e., before pyrolysis). This study can be of high importance for various applications, including membrane separations. Such properties are evaluated through pore structure characterization as well as Fourier transform infrared (FTIR), thermal gravimetric analysis (TGA), scanning electron microscopy (SEM), and adsorption capacity of nitrogen at a temperature of 77 K.

Materials and methods

Resorcinol (ACS, 99.98%, Alfa Aesar), formaldehyde (37% in water, Aldrich), sodium carbonate (anhydrous, ACS, Fisher), nitric acid (HNO_3 , 70.4%, Mallinckrodt), and acetone (optima, 99.6%, Fisher) were used as received. Ultra purified water produced from Milli-Q integral water purification system was used in the experiments.

Xerogels were prepared to cover a variety of the molar ratios of resorcinol-to-formaldehyde (R/F), resorcinol-to-water (R/W), and resorcinol-to-catalyst (R/C). Also, the initial solution pH was adjusted with diluted nitric acid and ammonium hydroxide at neutral or slightly acidic conditions. The curing temperature was fixed at 70 ± 1 °C. The conditions used for synthesizing the 16 gel samples are summarized in Table 1. The letters indicated under the “Sample ID” column in Table 1 will be used onward to refer to the corresponding conditions indicated in the same row. Resorcinol and sodium carbonate were weighted and mixed with ultrapure water in Erlenmeyer flasks and then stirred magnetically until all resorcinol and sodium carbonate are completely dissolved. Then, the specified amount of formaldehyde was added to the dissolved ingredients. After that, the solution pH values were adjusted to the desired value by using diluted nitric acid and ammonium hydroxide. RF solutions were then poured

Fig. 1 Schematic mechanism of polymerization reaction of resorcinol with formaldehyde



into polypropylene vials, sealed and placed in an oven at 70 ± 1 °C for 7 days. In order to prevent the dehydration of the gels, and to increase their cross-linking in the same time, 2% acetic acid was poured upon the gels surfaces after their solidification. Then, the vials were removed from the oven and allowed to cool to room temperature. The remnant solutions above the cured gels were then decanted and exchanged with acetone at room temperature. The samples were left in acetone at room temperature, and the remaining acetone is replaced with fresh acetone daily for 3 days. After the third day of solvent exchange, the

cured gels and the accompanying fresh acetone were placed in the oven at 50 ± 1 °C, and were kept for 2 days to dry at that condition [21].

Fourier transform infrared (FTIR) spectra were measured with ATI Genesis Series FTIR spectrophotometer using KBr pellet to ascertain the structure of RF xerogel samples. Spectra were acquired in wavenumbers between 4,000 and 400 cm^{-1} . TGA measurements were carried out with Perkin Elmer Pyris 6 TGA-Thermogravimetric Analyzer from ambient temperature up to 900 °C, with a heating rate of 10 °C/min under a nitrogen atmosphere.

Table 1 Synthesis conditions used to prepare the *R/F* gels

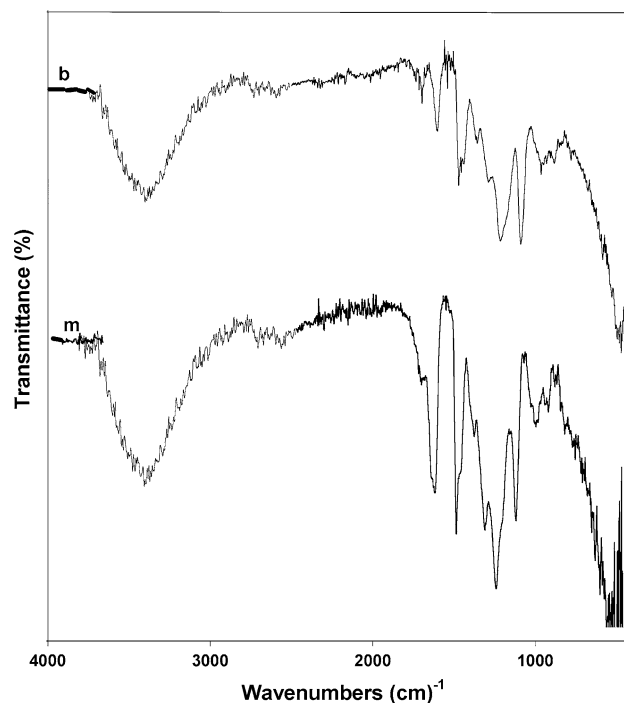
Sample ID	<i>R/W</i> (mol/mol)	<i>R/F</i> (mol/mol)	<i>R/C</i> (mol/mol)	pH
a	0.05	0.3	50	5.5
b	0.05	0.3	50	7.0
c	0.05	0.3	500	7.0
d	0.05	0.3	500	5.5
e	0.05	0.5	50	5.5
f	0.05	0.5	50	7.0
g	0.05	0.5	500	7.0
h	0.05	0.5	500	5.5
i	0.15	0.3	50	5.5
j	0.15	0.3	50	7.0
k	0.15	0.3	500	7.0
l	0.15	0.3	500	5.5
m	0.15	0.5	50	7.0
n	0.15	0.5	50	5.5
o	0.15	0.5	500	5.5
p	0.15	0.5	500	7.0

The morphology of xerogel samples was observed with a scanning electron microscope (SEM, Philips 515). The pore structures of the synthesized xerogels were measured using a Micromeritics ASAP-2420 surface area and porosity analyzer, which was used to estimate the surface areas, pore volumes, and pore size distributions of the prepared xerogel samples via measuring the nitrogen adsorption isotherms at 77 K and using built-in density functional theory calculations.

Results and discussion

FTIR spectra

Figure 2 illustrates sample FTIR spectra of selected RF xerogels samples “b” and “m”, as labeled on the corresponding spectra. Various infrared (IR) absorption peaks were evident of the presence of various functional groups presented in Fig. 1. For example, the IR absorption peaks at 294, 2874, and 1479 cm^{-1} were related to CH_2 stretching groups. The absorption peak at 1624 cm^{-1} was assigned to aromatic ring stretching vibrations. The broad peak at 3444 cm^{-1} was characteristic for OH stretching vibration groups in phenol. The IR peaks at 1222 and 1092 cm^{-1} were associated with C–O–C stretching vibrations of methylene ether bridges between resorcinol molecules. The IR peak at 1720 cm^{-1} , which associated C=O stretching of aldehyde was not observed. Consequently, it can be deduced that the sol–gel reaction was complete.

**Fig. 2** FTIR spectra for *R/F* xerogels samples “b” and “m”

TGA analysis

TGA and differential thermal gravimetric (DTG) plots were measured for selected xerogel samples, (b, c, m, and o). The TGA plots (Fig. 3a) illustrate the weight loss (%) of the RF xerogel samples versus temperature ($^{\circ}\text{C}$), and the derivative plots (Fig. 3b) illustrate that the significant weight losses (%) for all samples occurred at the decomposition temperatures of 72, 100, and 583 $^{\circ}\text{C}$, consequently. It was also observed from (Fig. 3a) that the decomposition temperatures for xerogel samples begin at 300 $^{\circ}\text{C}$ and end at 900 $^{\circ}\text{C}$. The sequence of thermal stability for RF xerogel samples is found to follow the order “ $m > o > b > c$.” This is due to the different xerogel preparation conditions (i.e., pH and *R/W*, *R/F*, and *R/C* molar ratios). The weight loss at 72 $^{\circ}\text{C}$ could be due to release of volatile compounds trapped into matrix of the dried xerogels. The weight loss at 100 $^{\circ}\text{C}$ is due to moisture loss and the percentage weight loss at 583 $^{\circ}\text{C}$ may be attributed to the decomposition of side or/and bridge functional groups within the xerogels.

Scanning electron microscope (SEM) micrographs

Figure 4 shows the SEM Micrographs for selected RF xerogel samples (e, j, m, and p). These selected SEM images demonstrate clear differences in the morphology of the RF xerogel samples. For example, samples “e” and

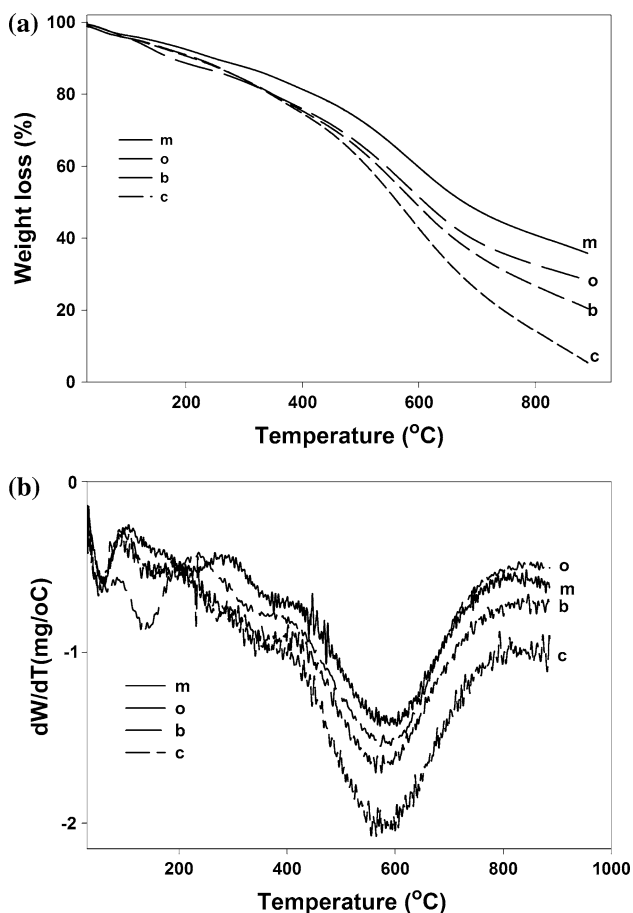


Fig. 3 Thermogravimetric analyses thermograms of xerogel samples “m, o, b, and c”. **a** and **b** show the TGA and DTG curves, respectively

“m” show big particles of $\sim 3 \mu\text{m}$ in diameter, which are interconnected with clear necks. On the other hand, samples “j” and “p” show very small particles, especially for sample “j.” The main difference between these two groups of samples is the R/C ratio, where samples “m, e, and j” have lower R/C ratios (higher catalyst concentrations) than sample “p” as shown in Table 1.

Structural characteristics

One of the most important features of RF gel materials is the resulting structural features corresponding to various synthesis conditions. To evaluate the effect of the studied synthesis conditions on the RF xerogels, their structural characteristics were measured to find out the average pore width, total pore volume, total surface area, and the adsorption capacity of nitrogen at 77 K. The measured characteristics for each sample are discussed in the following sections.

Effect of preparation conditions on pore size distributions

Figure 5 shows the variation of the cumulative volumes with the pore width for each of the RF xerogels which were prepared at different conditions. The increase in pore volume when increasing the pore width was obvious for xerogels samples “p, k, i, l, f, d, o, and j.” On the other hand, the remaining samples “a, b, c, e, g, h, n, and m” exhibited a very slight dependence of the cumulative pore volume with the increasing pore width. This indicates that these latter samples do not contain big pores that may contribute to increasing the cumulative pore volumes. The increasing behavior in cumulative volume in “p, k, i, l, f, d, o, and j” xerogel samples begins with pore width from 14 to 77 Å, which indicates the dominating pore size range for these samples. The plateau in xerogel samples start up with about 77–175 Å, which gives a sign that these samples include a negligible portion of pores in this range. The increase in cumulative pore volume happened again for all the previous xerogels except sample “l” which leveled off from 175 to 300 Å. Even though this sample has leveled off early compared to others, it has a big cumulative volumes at small pores widths. These changes in pore structures are assignable to different preparation condition of RF xerogels [11].

Effect of pore size on incremental volume

Figure 6 shows the incremental volume for each sample versus the corresponding pore widths. Figure 6a shows an overall view for pore widths up to 300 Å, and Fig. 6b shows a zoomed-in view of pore widths up to 100 Å. Overall, it was deduced that the pore structure of RF xerogel samples constitutes of three major pore size regions as shown in Fig. 6b. The first region ranges from 14 to 22 Å for samples “l, p, i, k, f, d, o, j, and n” in respective decreasing order. The second region ranges from 22 to 100 Å for samples “l, k, i, d, p, f, o, and j” in respective decreasing order. The third region, which is obvious in Fig. 6a, ranges from 100 to 300 Å for samples “p, i, f, d, o, and j” in respective decreasing order. This pore-region segregation character is very interesting for this kind of materials because it gives guiding signs to possible separation processes that can be achieved with such porous materials. For example, the pore sizes of the first region (between 14 and 22 Å) may become useful in the microfiltration processes of emulsions and colloids, synthetic drugs, herbicides, pesticides, etc. [22]. However, the pore sizes of the second region may become useful in microfiltration of cellular bacteria, polymers and starch, viruses, etc. [23]. Similarly, the pore sizes of the third region may be useful in separating lipoproteins, proteins,

Fig. 4 SEM morphologies of selected xerogels. The scale bar at the bottom of each image stands for a length of 10 μm

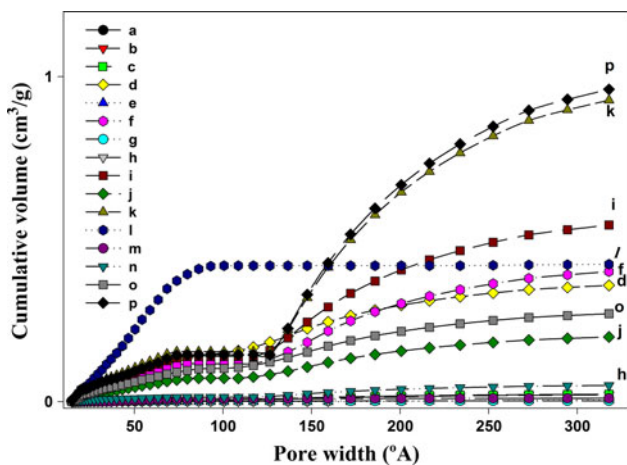
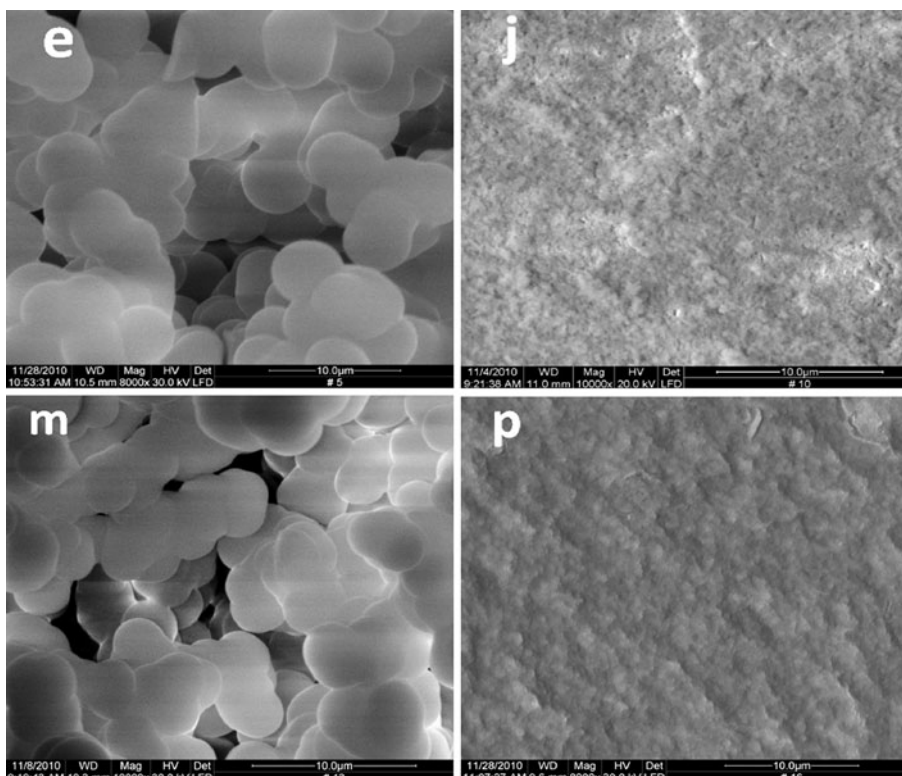


Fig. 5 Variation of cumulative volume with pore width for different R/F xerogels

enzymes, tobacco smoke, etc. [24]. The particle size distributions show that xerogel pores are among micro-, meso-, and macropore sizes. However, the major character is meso- and macropore sizes, whereas micropores are very few based on the preceding results.

Effect of pore size on cumulative area

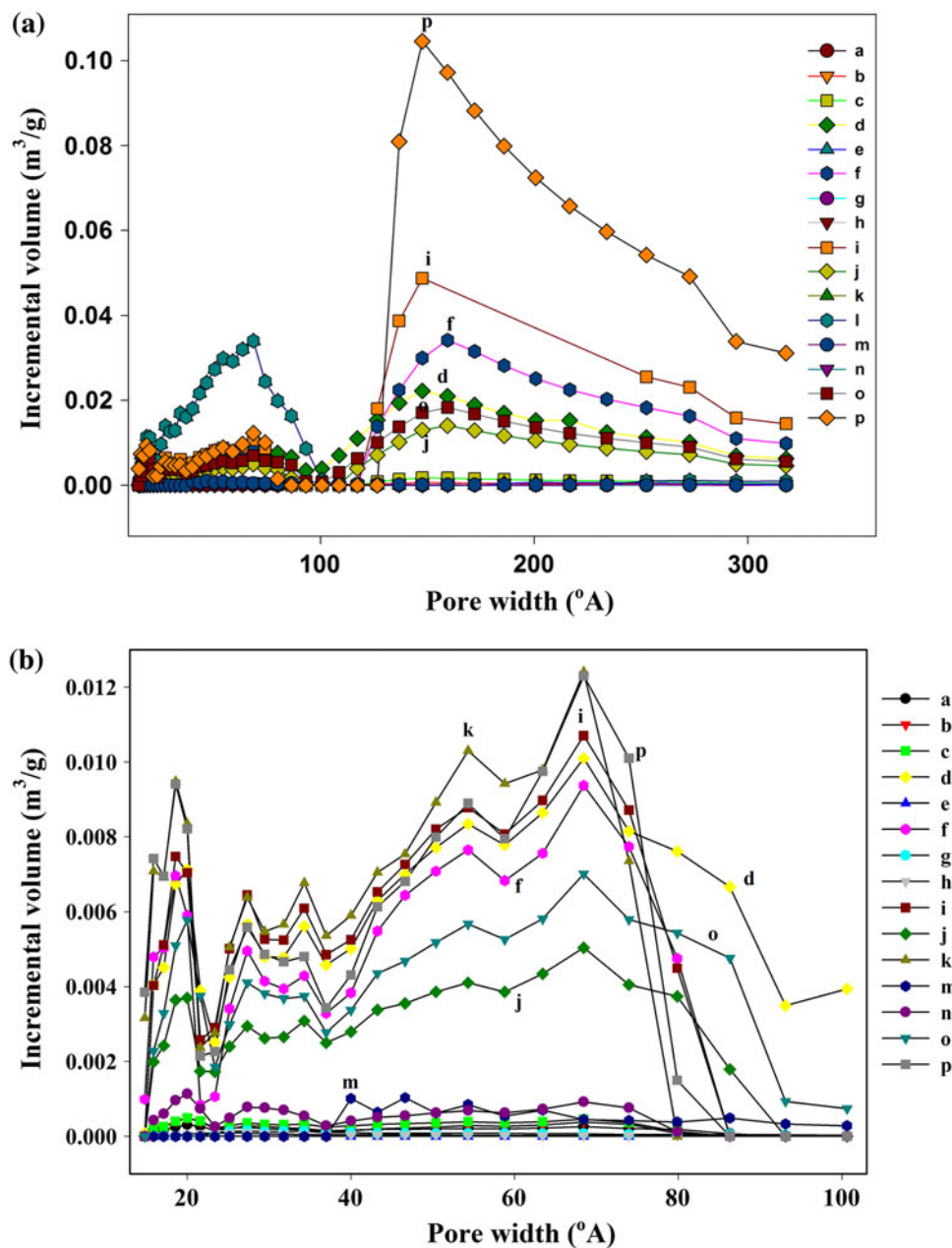
Figure 7 shows the variation of cumulative surface area of xerogels with pore widths. Overall, the trends of the cumulative surface area variations are identical to those of

the cumulative pore volume. Nonetheless, sample “l” showed a pronounced total surface area compared to the others which affirms the conclusion of this sample being rich in micropores. It was concluded from a previous result that these xerogels have three distinct pore structures; micro-, meso-, and macropore structure. But the major parts are meso- and macrostructures. Therefore, when mapping the xerogel structures, the results in Fig. 7 are consistent with those in Fig. 6.

Effect of synthesis conditions on the adsorption capacity of nitrogen at 77 K

In general, the extent of surface development and the nanoscale pore volume determine the adsorption capacity of such materials at high relative pressures through the pore-filling mechanism, whereas the surface area has a dominant effect on the adsorption process at very low relative pressures [25]. Figure 8 shows the measured adsorption isotherms of nitrogen on the RF xerogel samples at 77 K versus its relative pressure (actual pressure divided by vapor pressure). As explained previously, the major parts of xerogel pore structures are meso- and macropores, whereas the minor part is micropores. This conclusion is based on the results obtained from Figs. 5, 6, 7. Therefore, meso- and macropore volumes and surface areas control the adsorption process at high relative pressures. The adsorption capacities of nitrogen shoot up at relative

Fig. 6 Pore size distributions of the *R/F* xerogels in terms of incremental volume: **a** overall variations for pore widths up to 300 Å, **b** zoomed-in view for pore widths < 100 Å



pressures approaching one as shown in Fig. 8. This is believed to be due to capillary condensation which is known to occur in mesopores [26].

Factorial design analysis

A 2^4 full factorial design analysis of the effects of the studied factors and their two-level factor interactions on the maximum adsorption capacity, total pore volume and total surface area are presented in Fig. 9. The effects of these factors on the maximum amount adsorbed are shown in Fig. 9a and b, on the total pore volume in Fig. 9c and d, and on the total surface area in Fig. 9e–g. For a 75%

confidence level and sixteen degrees of freedom, the statistically significant effect of various factor or factor interactions are marked with a *t* value of 1.301 as indicated by the reference vertical line in the Pareto plots (Fig. 9a, c, and e).

Analyses of the effects of these factors on the maximum adsorption capacity and pore volume versus the synthesis conditions resulted in the Pareto charts shown in Fig. 9a and c, respectively. Both Figures show that the main factors ($A = R/W$ ratio, $B = R/F$ ratio, $C = R/C$ ratio, and $D = \text{pH}$) and their binary interactions (AB , AC , BC , AD , BD , and CD) exhibited noticeable effects on these properties, but with variable significances. However, only the

Fig. 7 Variation of cumulative surface areas with pore widths

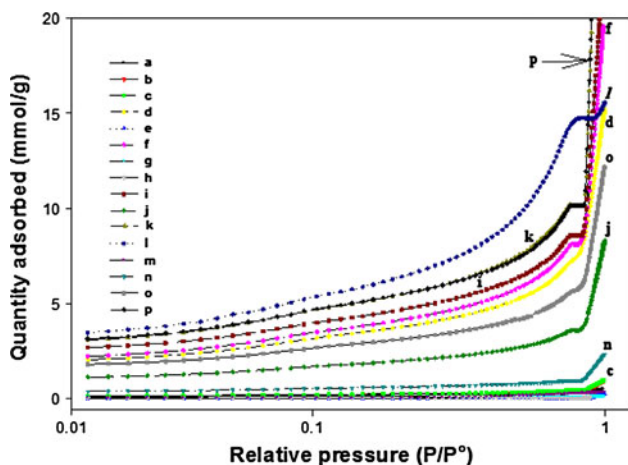
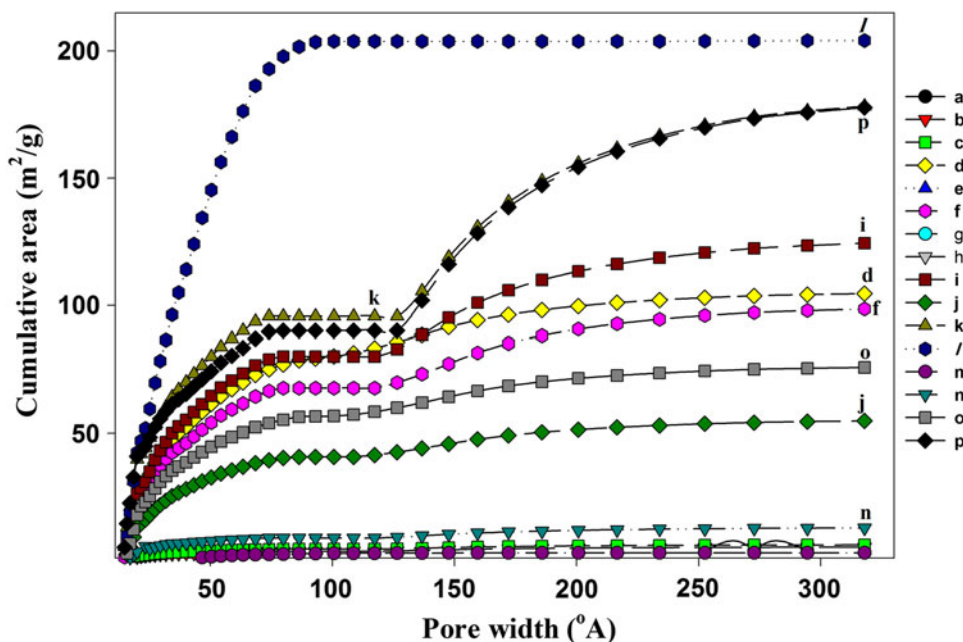


Fig. 8 Adsorption isotherms of nitrogen at 77 K on the *R/F* xerogels

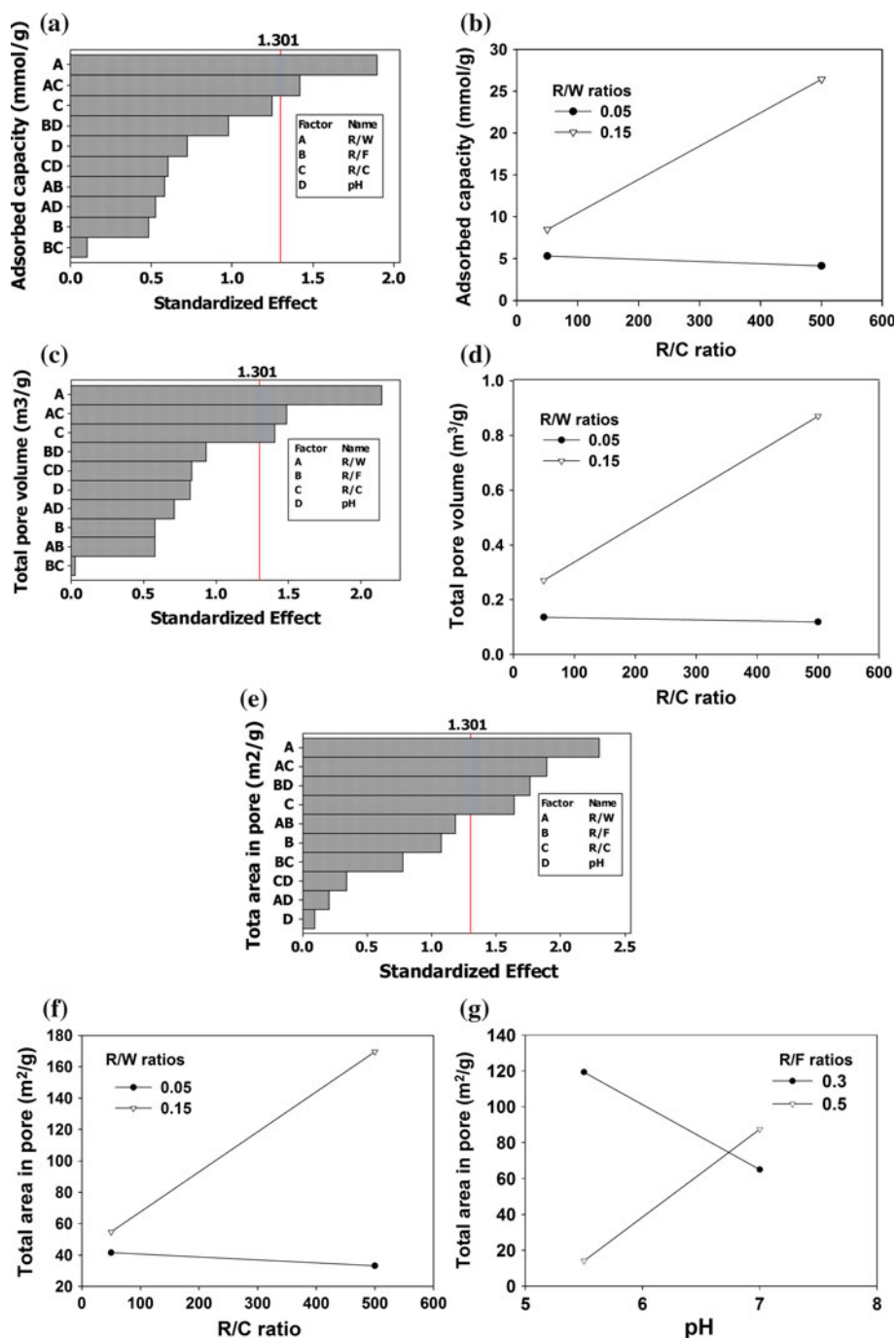
AC interaction (between the *R/W* and *R/C* ratios) had significant effects on the adsorption capacity and pore volume that extends beyond the reference line. The interaction plots for the adsorption capacity and total pore volume (Fig. 9b, d, respectively) show that the effect of these two factors (*R/W* and *R/C* ratio) is higher and more significant at high *R/W* ratio, especially when accompanied with high *R/C* ratio. Increasing the *R/W* ratio at low *R/C* ratio also increases the adsorption capacity and total pore volume, but to a smaller extent. On the other hand, low *R/W* ratio resulted in very small adsorption capacity and pore volume, regardless of *R/C* ratio.

Figure 9e shows that the most significant factors in determining the total surface area are the interaction

between *R/W* and *R/C* ratios (AC), followed by the interaction between *R/F* ratio and pH (BD). The AC interaction plot, which is presented in Fig. 9f, shows that the effects of *R/W* and *R/C* ratios on the total surface area are similar to those of the same factors on the adsorption capacity and total pore volume as discussed above. The BD interaction is statistically significant and shows significant effects of both the *R/F* ratio and the initial solution pH as shown in Fig. 9g. Reducing the initial solution pH increases the total surface area in case of low *R/F* ratio. On contrast, at high *R/F* ratio, the total surface area increases when increasing the initial solution pH value. These contrasting effects of the initial solution pH on the total surface area could indicate variable reaction mechanisms under various conditions as illustrated in Fig. 1. Nonetheless, the maximum total surface area in the first case (low *R/F* ratio and low pH) is significantly more than that of the latter case (high *R/F* ratio and high pH). This indicates that the cross-linking between monomers becomes more substantial in the case of excess formaldehyde and acidic conditions.

It is noteworthy that all the studied factors have noticeable effects on the characteristics of the synthesized xerogels as discussed in the previous sections. However, the interactions discussed in this section are only those which give statistical significances that fulfill the set confidence level of 75%. The effects of other factor (and factor interactions) are also being significant, but their effects are probably in a comparable order of magnitude to the corresponding experimental errors, which reduced the indicated statistical effect of their significances.

Fig. 9 Factorial design analysis for the effects of various synthesis conditions on the adsorption capacity (a, b), total pore volume (c, d), and total surface area (e–g). The standardized effects are shown in Pareto charts (a, c, and e); and the effects of significant factor interactions are shown in the corresponding interaction plots (b, d, f, and g)



Conclusions

Resorcinol–formaldehyde xerogels were synthesized successfully under various conditions (*R/W* molar ratio, *R/F* molar ratio, *R/C* molar ratio, and initial solution pH) at 70 °C. The resulting xerogels have satisfactorily high pore volumes and surface areas (up to 0.97 cm³/g and 200 m²/g). Xerogel samples were characterized by FTIR, TGA, and SEM techniques; and the structural properties were measured by a Micromeritics surface area analyzer. Full factorial design analyses experiments demonstrated a

statistically significant interaction between resorcinol-to-water and resorcinol-to-catalyst ratios. This interaction had influence on adsorption capacity, total pore volumes and total surface areas. Although the interaction between resorcinol-to-formaldehyde ratio and the initial solution pH had a lesser effect, it shows statistical significance on the total surface area. The pore structure of xerogels is found to be divided into three regions, micro-, meso-, and macropores. The presence of micropores in the xerogel structures is very small compared to those of meso- and macropores. The synthesized xerogels could be potentially used in

separation and adsorption processes dependent on pore volume and pore surface area that can be extracted from results presented in this study.

Acknowledgements This publication was made possible by the support of an NPRP grant from the QNRF. The statements made herein are solely the responsibility of the authors.

References

1. Mahata N, Pereira MFR, Suárez-García F, Martínez-Alonso A, Tascón JMD, Figueiredo JL (2008) *J Colloid Interface Sci* 324:150
2. Pekala RW (1989) *J Mater Sci* 24:3221. doi:[10.1007/BF01139044](https://doi.org/10.1007/BF01139044)
3. Liu B, Creager S (2010) *J Power Sources* 195:1812
4. Wen Y, Shen Z (2001) *Carbon* 39:2369
5. Czakkel O, Marthi K, Geissler E, László K (2005) *Microporous Mesoporous Mater* 86:124
6. Zhao H, Zhu Y, Li W, Hu H (2008) *New Carbon Mater* 23:361
7. Lee YJ, Jung JC, Yi J, Baeck S, Yoon JR, Song IK (2010) *Curr Appl Phys* 10:682
8. Li J, Wang X, Wang Y, Huang Q, Dai C, Gamboa S, Sebastian PJ (2008) *J Non-Cryst Solids* 354:19
9. Zheivot VI, Molchanov VV, Zaikovskii VI, Krivoruchko VN, Zaitseva NA, Shchuchkin MN (2010) *Microporous Mesoporous Mater* 130:7
10. Wang Z, Zhang X, Liu X, Lv M, Yang K, Meng J (2011) *Carbon* 49:161
11. Job N, Panariello F, Marien J, Crine M, Pirard JP, Léonard A (2006) *J Non-Cryst Solids* 352:24
12. Albert DF, Andrew GRs, Mendenhall RS, Bruno JW (2001) *J Non-Cryst Solids* 296:1
13. Job N, Panariello F, Crine M, Pirard JP, Léonard A (2007) *Colloids Surf A* 293:224
14. Shady SA (2009) *J Hazard Mater* 167:947
15. Al-Muhtaseb SA, Ritter JA (2003) *Adv Mater* 15:101
16. Brinker CJ, Scherer GW (1990) *Sol-gel science: the physics and chemistry of sol-gel processing*. Academic Press, London
17. Lin C, Ritter JA (1997) *Carbon* 35:1271
18. Zanto EJ, Al-Muhtaseb SA, Ritter JA (2002) *Ind Eng Chem Res* 41:3151
19. Matos I, Fernandes S, Guerreiro L, Barata S, Ramos AM, Vital J, Fonseca IM (2006) *Microporous Mesoporous Mater* 92:38
20. Horikawa T, Ono Y, Hayashi J, Muroyama K (2004) *Carbon* 42:2683
21. Hwang SW, Hyun HS (2004) *J Non-Cryst Solids* 347:238
22. Van der Bruggen B, Everaert K, Wilms W, Vandecasteele C (2001) *J Membr Sci* 193:239
23. Zhu B, Clifford DA, Chellam S (2005) *Water Res* 39:3098
24. Bierman EL, Hayes TL, Hawkins JN, Ewing AM, Lindgren FT (1966) *J Lipid Res* 7:65
25. Lee WH, Park JS, Sok JH, Reucroft PJ (2005) *Appl Surf Sci* 246:77
26. González-González JF, Alexandre-Franco M, González-García CM, Encinar-Martín JM, Bernalte-García A, Gómez-Serrano V (2009) *Powder Technol* 192:339